A dichotomy in group II Herbig disks: ALMA gas disk height measurements show both shadowed large vertically extended disks and compact flat disks

Stapper, L.M.; Hogerheijde, M.R.; Dishoeck, E.F. van; Paneque Carreño, T.P.

A&A 669, A158 (2023)
https://doi.org/10.1051/0004-6361/202245137

Astronomy & Astrophysics

A dichotomy in group II Herbig disks

ALMA gas disk height measurements show both shadowed large vertically extended disks and compact flat disks

L. M. Stapper[1], M. R. Hogerheijde[1,2], E. F. van Dishoeck[1,3], and T. Paneque-Carreño[1,4]

[1] Leiden Observatory, Leiden University, PO Box 9513, 2300 RA Leiden, The Netherlands
e-mail: stapper@strw.leidenuniv.nl
[2] Anton Pannekoek Institute for Astronomy, University of Amsterdam, PO Box 94249, 1090 GE Amsterdam, The Netherlands
[3] Max-Planck-Institut für Extraterrestrische Physik, Giessenbachstrasse 1, 85748 Garching, Germany
[4] European Southern Observatory, Karl-Schwarzschild-Str 2, 85748 Garching, Germany

Received 4 October 2022 / Accepted 19 November 2022

ABSTRACT

Context. Herbig stars can be classified as group I or group II depending on the shape of the far-infrared excess from the spectral energy distribution. This distinction may be evolutionary and related to the vertical structure of the Herbig disks.
Aims. Our aim is to determine the emission height of Herbig disks and compare the resulting vertical extent of both groups.
Methods. We used Atacama Large Millimeter/submillimeter Array (ALMA) Band 6 observations of ^{12}CO J = 2–1 emission lines at sufficient velocity (~0.3 km s^{-1}) and spatial resolution (~30 au) of eight Herbig disks (four group I and four group II sources) to determine the emission heights from channel maps generated via geometrical methods previously developed in other works.
Results. We find that all group I disks are vertically extended with a height to radius ratio of at least 0.25 and that for three of the disks, the gas emission profile can be traced out to 200–500 au. The group II disks are divided between MWC 480 and HD 163296, which have emission height profiles similar to the group I disks, and AK Sco and HD 142666, which are very flat (not exceeding a height of 10 au over the full extent traced) and more compact (<200 au in size). The brightness temperatures show no differences between the disks when the luminosity of the host star is accounted for.
Conclusions. Our findings agree with previous work that suggests group I disks are vertically extended and that group II disks are either large and self-shadowed or compact. Both MWC 480 and HD 163296 could be precursors of group I disks that have not yet formed a cavity that would allow for irradiation of the outer parts of the disk. The very flat disks, AK Sco and HD 142666, could have been caused by significant settling due to the advanced age of the disks (~20 instead of <10 Myr). The large differences in vertical structure are not reflected in the spectral energy distributions of these disks. More and deeper observations at higher spatial and velocity resolution are necessary to further characterize the Herbig subgroups.

Key words. protoplanetary disks – stars: early-type – stars: pre-main sequence – stars: variables: T Tauri, Herbig Ae/Be – submillimeter: planetary systems

1. Introduction

Herbig Ae/Be stars (e.g., Herbig 1960; Waters & Waelkens 1998) are pre-main-sequence stars of intermediate mass and spectral type between B and mid-F. The disks around Herbig stars (hereafter Herbig disks) have been found to be larger than those around T-Tauri stars (Acke et al. 2004; van der Marel & Mulders 2021; Stapper et al. 2022). This characteristic could explain why giant planets are more common around intermediate-mass main-sequence stars (e.g., Johnson et al. 2007; Fulton et al. 2021). The potential of forming a giant planet may be linked to the group I and II spectral energy distribution (SED) characterization of Herbig disks (Stapper et al. 2022). These two groups are based on the shape of the SED, specifically on the infrared (IR) excess (Meeus et al. 2001; Acke et al. 2009). While group II SEDs can be fitted with a single (power) law across the near-far IR wavelength range, group I SEDs require an additional blackbody component that dominates the far-IR emission. Based on these differences, group I disks are interpreted to be flaring disks (or vertically extended, i.e., increasing height with radius), while the group II disks are flat (i.e., constant height with radius) or self-shadowed (Meeus et al. 2001).

Originally, an evolutionary sequence from group I to group II was hypothesized, with grain growth and settling reducing the far-IR emission (Dullemond & Dominik 2004a,b, 2005). However, the evolution of the Herbig subgroups has been shown to be more complicated. Most, if not all, Herbig group I disks have been found to have inner cavities (Honda et al. 2012; Maaskant et al. 2013), which has given rise to the idea that the flux increase at longer wavelengths is due to an irradiated inner cavity wall. Consequently, an evolution from group I to group II was discarded, and instead, it was proposed that group II objects might eventually evolve into group I objects by means of the creation of an inner cavity (Maaskant et al. 2013; Menu et al. 2015).

However, the lack of scattered light from group II disks suggests that these disks may still be flat or self-shadowed disks (e.g., Garufi et al. 2017, 2022). This led Garufi et al. (2017) to propose that group II disks can either be self-shadowed large disks or small compact disks, which is in contrast to the group I disks, as they are all large and bright in both scattered

Table 1. Data and stellar parameters of each Herbig disk.

Group	Herbig disk	Vel. res. (km s^{-1})	Sp. res. ($''$)	rms (mJy beam^{-1})	Project ID	Dist. (pc)	$M_\star$ ($M_\odot$)	$L_\star$ ($L_\odot$)	Age (Myr)	Inc. (°)	PA (°)
I	HD 34282	0.2	0.27	4.6	2015.1.00192.S	306.5	<1.9	14.5	<20	60	117
	HD 97048	0.3	0.46	4.2	2015.1.00192.S	184.1	2.8	64.6	4	41	3
	HD 100453	0.3	0.25	3.5	2015.1.00192.S	103.6	1.6	6.2	19	30	140
	HD 100546	0.2	0.24	4.2	2016.1.00344.S	108.0	2.1	21.9	8	43	139
II	AK Sco	0.3	0.15	2.5	2016.1.00204.S	139.2	1.7	5.6	8	109	51
	HD 142666	0.35	0.13	1.6	2016.1.00484.L	145.5	1.8	13.5	9	62	162
	HD 163296	0.2	0.14	0.6	2018.1.01055.L	100.6	1.9	15.5	10	46	312
	MWC 480	0.2	0.3	1.2	2018.1.01055.L	155.2	1.9	16.6	8	–32	328

Notes. The stellar parameters are taken from Guzmán-Díaz et al. (2021). The following lists where the inclinations and position angles were taken from: AK Sco, Czekala et al. (2015); HD 142666, Huang et al. (2018); HD 163296, Izquierdo et al. (2022); MWC 480, Teague et al. (2021); HD 34282, van der Plas et al. (2017); HD 100453, Rosotti et al. (2020); HD 97048, Walsh et al. (2016); HD 100546, Pineda et al. (2019).

light (Garufi et al. 2014) and millimeter observations (Stapper et al. 2022). Consequently, the question arises of whether the differences in vertical disk height are also present in the gas.

In recent years, the high velocity and spatial resolution of the Atacama Large Millimeter/submillimeter Array (ALMA) has allowed for the vertical structure of mid-inclination protoplanetary disks to be characterized (e.g., Pinte et al. 2018; Rich et al. 2021; Law et al. 2021, 2022; Paneque-Carreño et al. 2021, 2022, 2023), increasing the variety of disks that can be studied in addition to edge-on disks (e.g., Podio et al. 2020; Villenave et al. 2020). The emission heights of different molecules (e.g., Law et al. 2021) and asymmetries in the vertical emission of CO in a disk (Paneque-Carreño et al. 2021) have been found. In this paper, we apply the technique of Pinte et al. (2018) as implemented by Paneque-Carreño et al. (2023) on both group I and group II disks to determine the emission heights of ^{12}CO and see if there are any differences present between the two groups.

Section 2 presents the targets and how they were selected and imaged. Section 3.1 shows the extracted disk heights, and Sect. 3.2 shows the temperature maps of each disk. The results are discussed in the context of group I versus group II in Sect. 4.1 and in relation to the age of the very flat disks in Sect. 4.2. Lastly, in Sect. 5, the conclusions are summarized.

2. Sample selection and data reduction

In recent years, many Herbig disks have been observed with ALMA (for a recent compilation, see Stapper et al. 2022). Some of these data are deep, high-resolution observations. These data were either included in ALMA Large Programs, such as MAPS (Öberg et al. 2021) and DSHARP (Andrews et al. 2018), or studied separately. We selected our sample based on the available data in the ALMA archive[1] (Stapper et al. 2022). To be able to determine the emission heights of a disk, the data and the disk must meet several requirements. First, an inclination of at least 30° is needed to reliably extract the surface emitting heights (Law et al. 2021). Second, a certain level of velocity resolution is necessary to adequately trace the isovelocity curves in the selected channels. In general, a velocity resolution of at least ~0.3 km s^{-1} is necessary. Lastly, sufficient spatial resolution is necessary to distinguish both the nearside and the far side of the disk (for systematics, see Pinte et al. 2018; Paneque-Carreño et al. 2022). For our sources, this came down to ~30 au. To properly trace the vertical extent of the Herbig disks, we used ^{12}CO J = 2–1 observations. These requirements left us with eight data sets in total: four for group I and four for group II disks (see Table 1). The SEDs of these disks are shown in Appendix A and clearly show the distinguishing features of both groups. We note that this technique of determining the vertical extent of the disk traces the $\tau = 1$ line rather than the scale height of the gas. Paneque-Carreño et al. (2023) have shown that the ratio between the traced emission height and the gas scale height is generally a factor of two to five.

To obtain well-defined upper surfaces, ^{12}CO observations toward the eight disks were used. For HD 163296 and MWC 480, the imaged ^{12}CO data sets from the MAPS Large Program were used (see Czekala et al. 2021 for the specifics on the imaging). All other data were imaged using the `Common Astronomy Software Applications` (CASA), application version 5.8.0 (McMullin et al. 2007). For all data sets, the data were either binned by a factor of two in velocity, to increase the sensitivity, or the native velocity resolution was used. After subtracting the continuum using `uvcontsub` (which was not done for the temperature maps shown in Sect. 3.2), the data were imaged using the `multiscale` algorithm. The scales used were 0 (point source), 1, 2, 5, 10, and 15 times the size of the beam in pixels (~5 pixels). A Briggs robust weighting of 0.5 was used. For HD 142666 a *uv* taper of 0.08″ was applied to increase the beam size for better extraction of the emission surface heights. These steps resulted in the image parameters listed in Table 1. The velocity integrated maps of ^{12}CO can be found in Fig. 1 together with the Band 6 or 7 continuum images of each disk.

To obtain the emitting surface heights of the ^{12}CO emission, the technique set out in Pinte et al. (2018) was employed. Using geometric relations and assuming Keplerian rotation, the emission height can be retrieved. We used the same implementation of this technique as Paneque-Carreño et al. (2021, 2022, 2023), who made the distinction between the upper and lower emission surfaces visually through the use of hand-drawn masks with `ALFAHOR` (ALgorithm For Accurate H/R; Paneque-Carreño et al. 2023, see Appendix B). This approach limits contamination between the different surfaces, resulting in a cleaner retrieval of the emission surfaces. The extracted data points were averaged in bins of 20 au in size with an uncertainty corresponding to the standard deviation of the data points in that bin. The distances used and other stellar parameters can be found in Table 1. The resulting hand-drawn masks and extracted points are shown in the figures of Appendix B.

[1] https://almascience.eso.org/asax/

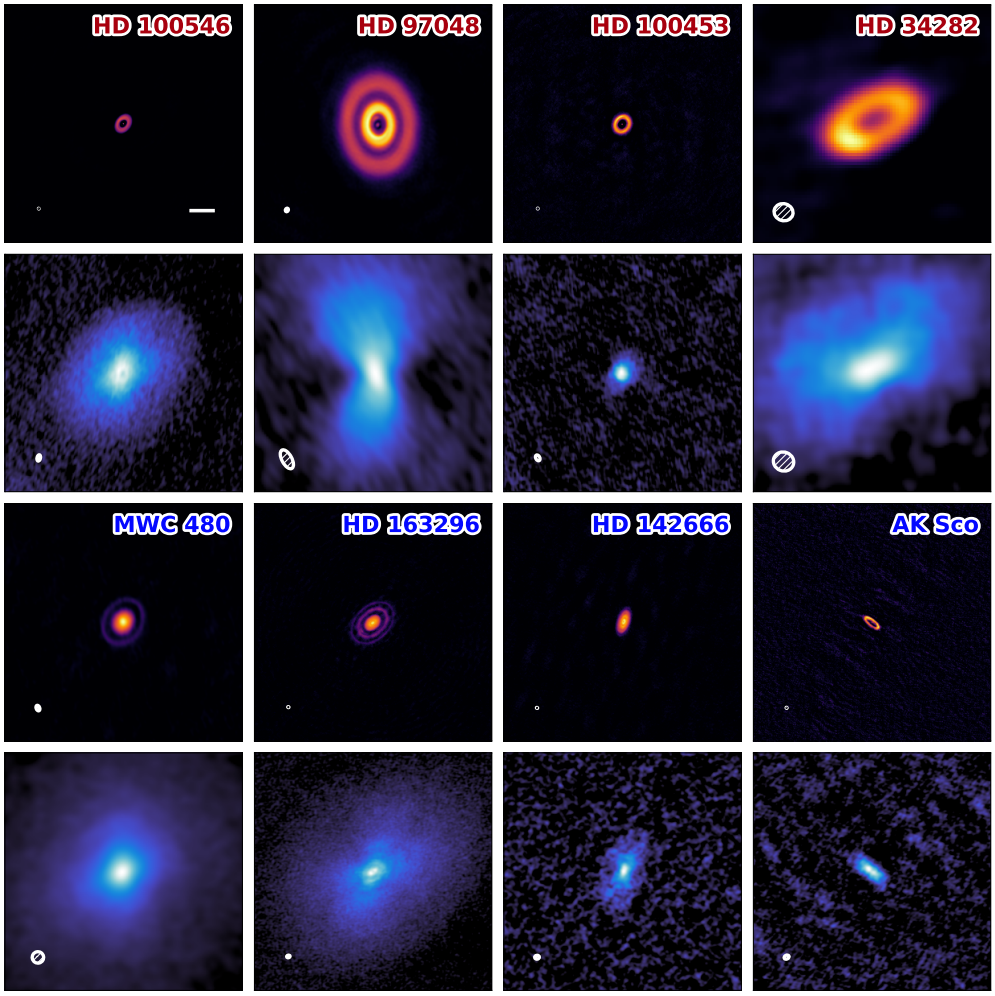

Fig. 1. Continuum and ^{12}CO velocity integrated (moment 0) maps of the group I disks (top two rows) and group II disks (bottom two rows). Each image is 1000 × 1000 au in size; additionally, a bar of 100 au in size is shown in the top-left panel. In the bottom-left corner of each image, the size of the beam is shown. The moment 0 maps use a 3σ clip and only include channels with disk emission. To make the outer regions of the disks more visible, a power-law normalization was used.

An exponentially tapered power law was fitted to each profile in order to easily compare between disks and other works. We followed Law et al. (2021) in using the following expression:

$$z(r) = z_0 \times \left(\frac{r}{1''}\right)^{\phi} \times \exp\left(-\left[\frac{r}{r_{\rm taper}}\right]^{\psi}\right), \quad (1)$$

where z is the vertical height of the surface emission, r is the radius of the profile, and $z0$ and $r_{\rm taper}$ are related to the size of the disk in the vertical and radial direction, respectively. All units are in arcseconds. In order to fit Eq. (1), we used the `curve_fit` function from `SciPy` (Virtanen et al. 2020) to do a nonlinear least-squares fit to the retrieved binned emission surfaces. Bins with only one point were excluded. Lastly, for additional visual aid in identifying whether the disks are vertically extended or flat, Appendix C presents the velocity maps of each disk.

3. Results

3.1. Disk heights

The continuum and the ^{12}CO line observations presented in Fig. 1 already show a large variety of structures and sizes regarding the disks in this work. Both HD 97048 and HD 34282 each show a large dust and gas disk extent. The dark regions in the ^{12}CO observations of HD 97048 are due to foreground cloud absorption. For the group I disks, all disks except HD 100453 are large in gas. Among the group II disks, HD 142666 and AK Sco are smaller compared to the other disks. The continuum of all the disks shows substructure, and half of the disks show a single dust ring, while the others show multiple rings.

Figure 2 presents the extracted height profiles for the eight disks. The top four panels show the group I disks, and the bottom four panels show the group II disks. In general, the heights of most of the disks are at a $z/r \sim 0.25$. All group I disks have a z/r of at least 0.25, either in large parts of the disk, such as HD 100546 or HD 97048, or at small radii only (HD 100453). MWC 480 and HD 163296 belong to group II and are vertically very similar to the group I disks. Both disks have a $z/r \sim 0.25$ and have gas disk sizes of around 500 au. In contrast, AK Sco and HD 142666 are flat and relatively small, only going out to 200 au. We will now discuss each disk separately.

While having similar or worse spatial resolution compared to the other disks, HD 34282 is limited by the resolution of the data, as its source was the farthest away (306.5 pc; see Guzmán-Díaz et al. 2021 or Table 1). For the inner 100 au, the far sides and the near sides of the disk cannot be separated from each other, making it impossible to sample the emission height at

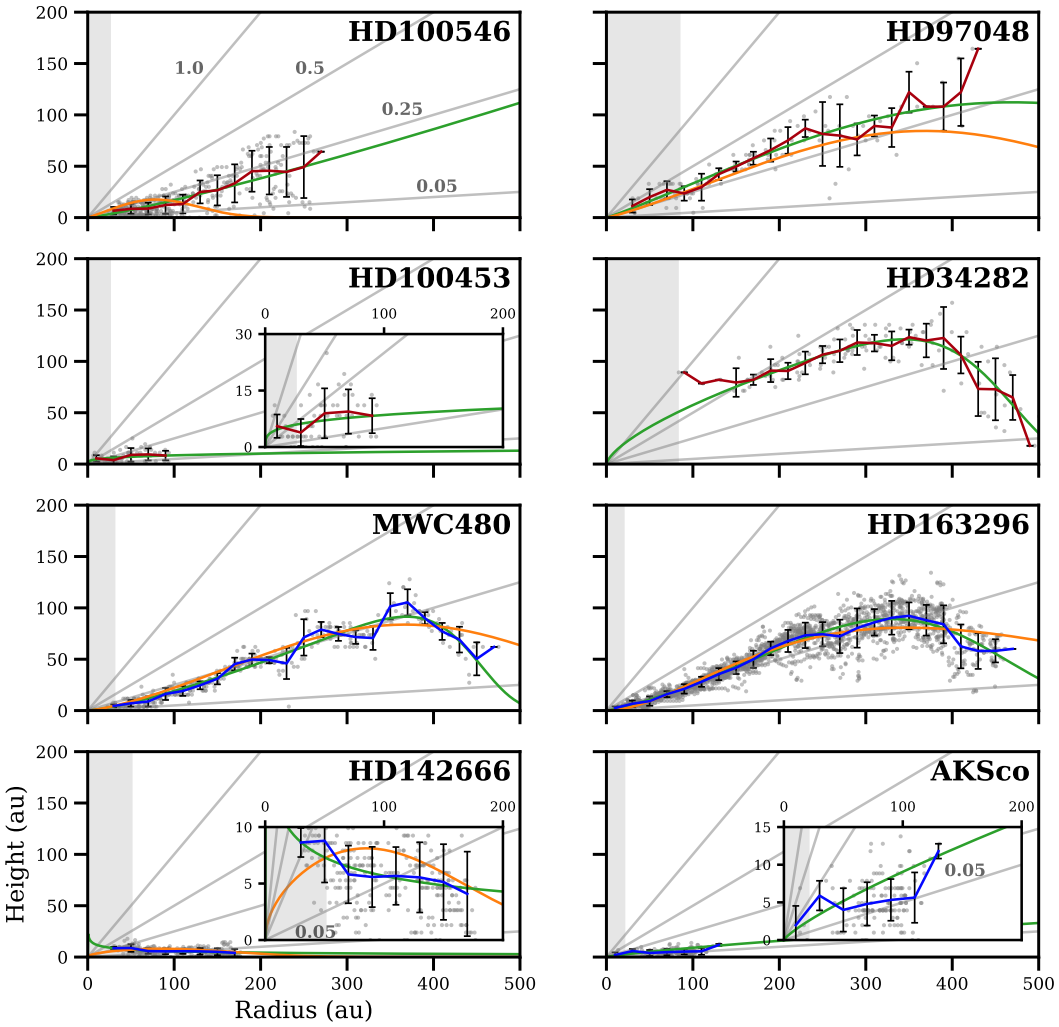

Fig. 2. Height profiles of the group I disks (top four panels) and group II disks (bottom four panels). The gray lines indicate the 1.0, 0.5, 0.25, and 0.05 height to radius ratios. The gray scatter is the extracted points from the channel maps, and the line shows the mean value of the scatter in bins of 20 au in size. The error bars indicate the standard deviation of the scatter in each bin. The fitted profiles are shown as green lines and are compared to the orange profiles from Law et al. (2021) for HD 163296 and MWC 480, Law et al. (2022) for HD 142666 and HD 100546, and Rich et al. (2021) for HD 97048. The gray-shaded regions indicate the size of the major axis of the beam.

these radii (see Fig. B.4). The part that is well sampled shows a vertically extended disk going as high as $z/r \sim 0.5$. In the case of HD 34282, the tapered power-law fit shows that at small radii the disk could go above $z/r \sim 0.5$, which is higher than what is found in most disks (e.g., Law et al. 2022).

In our sample, HD 97048 is also a high vertically extended disk, with a z/r out to 0.33. Although we did not probe the turnover at the large radii seen in many of the disks, we found that the emission originates from higher z/r regions in comparison to what Rich et al. (2021) found. While the inner region is again limited by the spatial resolution of the data, the profile is above a z/r of 0.25 at regions close to the mid-plane. The z/r values close to the mid-plane of the best fit correspond well with those of Rich et al. (2021), while the outer regions mainly contribute to the difference between the two fits. The data lack samples at lower velocities close to the system velocity (see Fig. C.1) due to foreground cloud absorption, which reduces the number of sampled heights in Fig. 2. For HD 100546, we were able to probe the emission heights to a larger radius than what was found by Law et al. (2022). However, no clear turnover was detected at these larger radii up to where we sampled the surface. The disk clearly follows a $z/r \sim 0.25$.

When fitting the exponentially tapered power law to the height profiles of MWC 480 and HD 163296, we found a steeper drop-off at large radii compared to what Law et al. (2021) found. This difference was due to our ability to better separate the lower and upper emission surfaces by drawing masks, which would have otherwise contaminated the overall inferred profile. At smaller separations, our relations agree with what Law et al. (2021) found, while due to a better sampling at larger separations, the relations start to differ at larger radii, resulting in a steeper drop.

For HD 142666, we found a very flat disk, similar to the disk height found by Law et al. (2022), but there are differences at small radii. In addition to HD 142666, we found a second very flat disk: AK Sco. Both of these disks are also the smallest disks in the sample of this work.

3.2. Disk temperatures

One would expect that these large differences in the height of the emitting layer would be reflected in the temperature of the emitting gas. To examine whether this is indeed the case, temperature maps of the disks were made, see Fig. 3. These maps

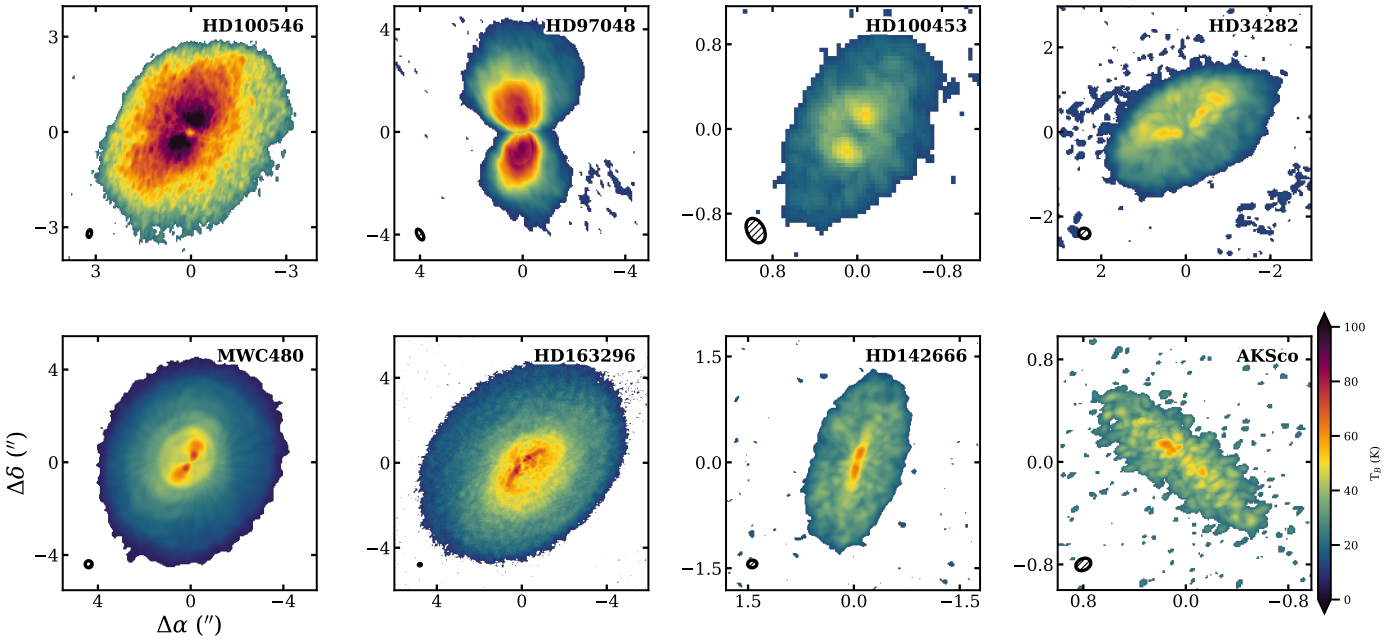

Fig. 3. Temperature maps of the eight disks, determined using the Planck law. The top and bottom rows show the group I and II disks, respectively. Each image is clipped at an S/N of 3. The size of the beam is shown in the bottom-left corner.

were made with `bettermoments` using a clip of 3×S/N and the full Planck expression. A radial cut along the disks' major axes that follows the projected fitted height profiles of the temperature maps can be found in the left column of Fig. 4. Each disk shows a decrease in temperature close to the star due to beam dilution, as the emitting region shrinks and no longer fills the beam (e.g., Leemker et al. 2022). Also, for HD 142666, the relatively low velocity resolution can lower the inferred temperature by under-resolving the line. Both Figs. 3 and 4 show large differences between temperatures of individual disks. However, no clear trend is present between the group I and group II sources, and there are disks from both groups that show very similar temperature profiles. For example, HD 100453, AK Sco, and HD 142666 are relatively cold, and HD 34282, HD 163296, and MWC 480 are relatively warm. The only clear outliers are HD 100546 and HD 97048, which are much warmer in the region out to 450 au compared to the other disks.

We might expect that these differences in temperature are due to the relative vertical extent of the disks. The right column of Fig. 4 shows radial cuts of the temperature maps where the temperature is scaled by the stellar luminosity as $\sim(L_\star/L_\odot)^{1/4}$ (following the dust temperature scaling presented in Andrews et al. 2013). This scaling removes the effect of the central star on the temperature of the disk. As presented in Table 1, both HD 100546 and HD 97048 are the most luminous stars in our sample and, compared to the less luminous stars, significantly increased the relative disk temperatures. When the scaling is applied, the relative disk temperatures become noticeably more similar. Most notably, the temperature profile of HD 97048 becomes almost identical to the profiles of HD 34282, MWC 480, and HD 163296. Consequently, the disk temperatures are as one would expect for their luminosity and size. Hence, we do not find a difference in temperature between the group I and group II sources despite differences in vertical extent.

Fedele et al. (2016) modeled Herbig Ae disks based on *Herschel*/HIFI high-J CO line profiles and determined the radial gas temperature structure for, among others, different vertically extended disks. They found that for a z/r between 0.01 and 0.3, the gas temperature is independent of the vertical extent of the disk and that the differences only start in higher layers probed by (very) high-J CO lines. Given that our ^{12}CO emission surfaces are from $z/r \sim 0.3$ and lower, our results fall in line with these models.

4. Discussion

4.1. Group I versus group II

The different Herbig disk groups were originally interpreted as group I being made up of flaring disks and group II being made up of flat or self-shadowed disks, with an evolution from group I to group II via dust settling. As outlined in Sect. 1, this view has become more complicated. Based on scattered light imaging, Garufi et al. (2017) proposed that group II disks can be divided into objects with large, shadowed disks and objects with small disks. Both result in a low far-IR flux. The shadowed disks could evolve into group I disks by creating an inner cavity, thus removing the part of the disk casting the shadow. Recent studies have shown a high occurrence rate of cavities in group I disks, in both gas and dust (e.g., Menu et al. 2015; van der Plas et al. 2015).

Most group I disks are large vertically extended disks. For the disks in group II, there is a clear difference between two sets of disks (e.g., MWC 480 and HD 163296 versus HD 142666 and AK Sco). The former are indistinguishable from the group I disks in our sample regarding both their size and the vertical extent of the disk, while the latter are more compact and flat.

These two sets of disks coincide with the proposed distinction between compact and self-shadowed disks within group II by Garufi et al. (2017). The analogous height profiles of MWC 480 and HD 163296 compared to the group I disks suggest that they are precursors of the group I disks, as Garufi et al. (2017) suggest for HD 163296. These disks are shadowed due to an inner disk that keeps the outer regions cool, which results in a group II SED. Once a cavity forms, the shadowing disappears, and a group I disk is formed. Throughout this evolution,

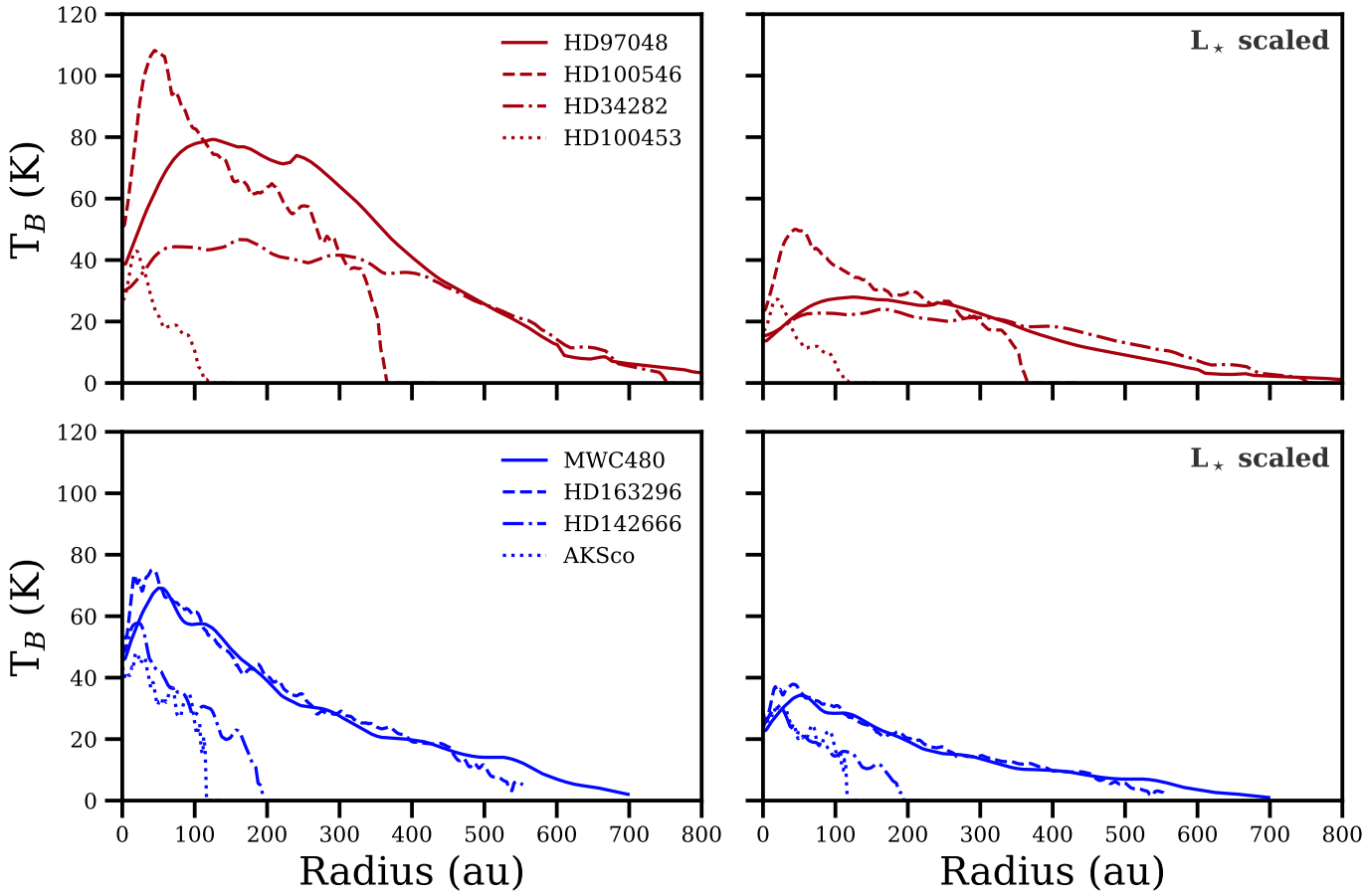

Fig. 4. Radial cuts of the temperature maps in Fig. 3 along the major axes of the disks and the projected emission surface fit shown in Fig. 2. The radial cuts are colored by group: group I (red, top row) and group II (blue, bottom row). The legend is ordered by stellar luminosity. The right panels show the temperature scaled by the stellar luminosity as $T \sim (L_\star/L_\odot)^{1/4}$ from Andrews et al. (2013).

the height profile of the disk stays the same. The puzzling aspect is that a higher temperature should result in a more vertically extended disk, but this was not observed. So there may be a (unrelated) trend occurring at the same time that results in a flatter disk that counteracts the effect of the larger illumination. The two flatter disks in our sample are also the most compact, and such a flat disk also result in a group II SED.

Hence, two types of group II disks can be distinguished. On the one hand are the disks that will eventually evolve into group I disks with very similar radial and vertical structures but with an inner disk that shadows the outer disk. And on the other hand are disks that are very flat and never develop an inner cavity that would expose the outer disk to heating.

We note that no differences between the vertically extended but shadowed and vertically flat disks are present in the SEDs of the group II disks (see Appendix A). As shown in Garufi et al. (2017, 2022), in general, multiple tracers are necessary to fully characterize a Herbig disk, one of which is the ability to spatially resolve the disk.

4.2. Old flat group II disks

Both AK Sco and HD 142666 are very flat disks compared to the other disks in our sample. What could cause such a flat disk?

The ages of these disks are not well determined and have a significant range of possible values. In Table 1 for instance, an age of 7.8 Myr is cited for AK Sco (Guzmán-Díaz et al. 2021). However, others give ranges of values from lower limits, from 12 Myr (Garufi et al. 2022) to 18 Myr (Czekala et al. 2015). While not present in this work due to too low spectral resolution observations, HD 9672 (or 49 Ceti) is a group II Herbig disk but is also considered to be a debris disk (e.g., Moór et al. 2019). The secondary dust in the debris disk, which is expected to have a low-scale height, could cause the group II classification. At the advanced age of these disks, the PAHs and small dust grains in the higher regions of the disk may have been removed. This in turn would lower the gas temperature and decrease the gas scale height. Hence, while they are not debris disks, the flat disks AK Sco and HD 142666 may have had significantly more evolution (dust settling and thus a decrease of the gas scale height) than one would assume based on the ages mentioned in Table 1.

5. Conclusion

In this work we determined the emission heights of eight Herbig disks, four group I disks (HD 100546, HD 97048, HD 100453, and HD 34282) and four group II disks (MWC 480, HD 163296, HD 142666, and AK Sco), following the classification of Meeus et al. (2001). With these emission heights, we tested the interpretation that group I disks are vertically extended irradiated disks and group II disks are self-shadowed or flat disks. The following conclusions have been made:

1. All but one of the group I disks are large (>200 au) and have $z/r \sim 0.25$. The exception is HD 100453, which has the same z/r as the other group I disks but is traced to a smaller radii.

2. Two of the group II disks (MWC 480 and HD 163296) have emission height profiles that are indistinguishable from those of the group I disks.
3. There are two very flat disks among the group II disks (HD 142666 and AK Sco). The emission heights of these very flat disks are below 10 au over the full extent of the traced disk (out to 200 au).
4. The temperatures reveal no significant differences between the disks when scaled based on the luminosity of the star despite differences in vertical extent.
5. Our findings correspond with the proposed scenario of Garufi et al. (2017), where some group II disks are self-shadowed and will evolve into a group I disk by forming a cavity that causes the outer disk to be irradiated (MWC 480 and HD 163296), while other group II disks are small and flat (AK Sco and HD 142666).
6. No significant differences are present between the SEDs of the flat and the vertically extended group II disks. Hence, resolved observations play a key role in fully characterizing the different Herbig disk populations.

The small source sample of only four objects in each SED group with available ALMA data of sufficient quality shows that more observations of sufficient S/N and resolution, both spatial and kinematic, are needed. Future studies with a larger sample must be done in order to place our reported dichotomy in gas disk heights on a firm statistical footing.

Acknowledgements. The research of LMS is supported by the Netherlands Research School for Astronomy (NOVA). This paper makes use of the following ALMA data: 2015.1.00192.S, 2016.1.00344.S, 2016.1.00204.S, 2016.1.00484.L, 2018.1.01055.L. ALMA is a partnership of ESO (representing its member states), NSF (USA) and NINS (Japan), together with NRC (Canada), MOST and ASIAA (Taiwan), and KASI (Republic of Korea), in cooperation with the Republic of Chile. The Joint ALMA Observatory is operated by ESO, AUI/NRAO and NAOJ. This work makes use of the following software: the Common Astronomy Software Applications (CASA) package (McMullin et al. 2007), Python version 3.9, alfahor (Paneque-Carreño et al. 2023), astropy (Astropy Collaboration 2013, 2018), bettermoments (Teague et al. 2018), matplotlib (Hunter 2007), numpy (Harris et al. 2020) and scipy (Virtanen et al. 2020). Our thanks goes to the European ARC node in the Netherlands (ALLEGRO) for their support with the calibration and imaging of the data. Lastly, we thank the referee for their insightful comments which have improved this paper.

References

Acke, B., van den Ancker, M. E., Dullemond, C. P., van Boekel, R., & Waters, L. B. F. M. 2004, A&A, 422, 621
Acke, B., Min, M., van den Ancker, M. E., et al. 2009, A&A, 502, L17
Andrews, S. M., Rosenfeld, K. A., Kraus, A. L., & Wilner, D. J. 2013, ApJ, 771, 129
Andrews, S. M., Huang, J., Pérez, L. M., et al. 2018, ApJ, 869, L41
Astropy Collaboration (Robitaille, T. P., et al.) 2013, A&A, 558, A33
Astropy Collaboration (Price-Whelan, A. M., et al.) 2018, AJ, 156, 123
Bessell, M. S. 1979, PASP, 91, 589
Cutri, R. M., et al. 2012, VizieR Online Data Catalog: II/311
Czekala, I., Andrews, S. M., Jensen, E. L. N., et al. 2015, ApJ, 806, 154
Czekala, I., Loomis, R. A., Teague, R., et al. 2021, ApJS, 257, 2
Dullemond, C. P., & Dominik, C. 2004a, A&A, 417, 159
Dullemond, C. P., & Dominik, C. 2004b, A&A, 421, 1075
Dullemond, C. P., & Dominik, C. 2005, A&A, 434, 971
ESA 1997, ESA Special Publication, 1200, The HIPPARCOS and TYCHO catalogues. Astrometric and photometric star catalogues derived from the ESA HIPPARCOS Space Astrometry Mission
Fedele, D., van Dishoeck, E. F., Kama, M., Bruderer, S., & Hogerheijde, M. R. 2016, A&A, 591, A95
Fulton, B. J., Rosenthal, L. J., Hirsch, L. A., et al. 2021, ApJS, 255, 14
Gaia Collaboration 2020, VizieR Online Data Catalog: I/350
Garufi, A., Quanz, S. P., Schmid, H. M., et al. 2014, A&A, 568, A40
Garufi, A., Meeus, G., Benisty, M., et al. 2017, A&A, 603, A21
Garufi, A., Dominik, C., Ginski, C., et al. 2022, A&A, 658, A137
Guzmán-Díaz, J., Mendigutía, I., Montesinos, B., et al. 2021, A&A, 650, A182
Harris, C. R., Millman, K. J., van der Walt, S. J., et al. 2020, Nature, 585, 357
Herbig, G. H. 1960, ApJS, 4, 337
Hindsley, R. B., & Harrington, R. S. 1994, AJ, 107, 280
Honda, M., Maaskant, K., Okamoto, Y. K., et al. 2012, ApJ, 752, 143
Huang, J., Andrews, S. M., Dullemond, C. P., et al. 2018, ApJ, 869, L42
Hunter, J. D. 2007, Comput. Sci. Eng., 9, 90
Ishihara, D., Onaka, T., Kataza, H., et al. 2010, A&A, 514, A1
Izquierdo, A. F., Facchini, S., Rosotti, G. P., van Dishoeck, E. F., & Testi, L. 2022, ApJ, 928, 2
Jensen, E. L. N., Mathieu, R. D., & Fuller, G. A. 1996, ApJ, 458, 312
Johnson, J. A., Butler, R. P., Marcy, G. W., et al. 2007, ApJ, 670, 833
Khalafinejad, S., Maaskant, K. M., Mariñas, N., & Tielens, A. G. G. M. 2016, A&A, 587, A62
Law, C. J., Teague, R., Loomis, R. A., et al. 2021, ApJS, 257, 4
Law, C. J., Crystian, S., Teague, R., et al. 2022, ApJ, 932, 114
Leemker, M., Booth, A. S., van Dishoeck, E. F., et al. 2022, A&A, 663, A23
Maaskant, K. M., Honda, M., Waters, L. B. F. M., et al. 2013, A&A, 555, A64
McMullin, J. P., Waters, B., Schiebel, D., Young, W., & Golap, K. 2007, in Astronomical Society of the Pacific Conference Series, 376, Astronomical Data Analysis Software and Systems XVI, eds. R. A. Shaw, F. Hill, & D. J. Bell, 127
Meeus, G., Waters, L. B. F. M., Bouwman, J., et al. 2001, A&A, 365, 476
Menu, J., van Boekel, R., Henning, T., et al. 2015, A&A, 581, A107
Moór, A., Kral, Q., Ábrahám, P., et al. 2019, ApJ, 884, 108
Öberg, K. I., Guzmán, V. V., Walsh, C., et al. 2021, ApJS, 257, 1
Paneque-Carreño, T., Pérez, L. M., Benisty, M., et al. 2021, ApJ, 914, 88
Paneque-Carreño, T., Miotello, A., van Dishoeck, E. F., et al. 2022, A&A, 666, A168
Paneque-Carreño, T., Miotello, A., van Dishoeck, E. F., et al. 2023, A&A, 669, A126
Pineda, J. E., Szulágyi, J., Quanz, S. P., et al. 2019, ApJ, 871, 48
Pinte, C., Price, D. J., Ménard, F., et al. 2018, ApJ, 860, L13
Podio, L., Garufi, A., Codella, C., et al. 2020, A&A, 642, L7
Rich, E. A., Teague, R., Monnier, J. D., et al. 2021, ApJ, 913, 138
Rosotti, G. P., Benisty, M., Juhász, A., et al. 2020, MNRAS, 491, 1335
Stapper, L. M., Hogerheijde, M. R., van Dishoeck, E. F., & Mentel, R. 2022, A&A, 658, A112
Teague, R., Bae, J., Bergin, E. A., Birnstiel, T., & Foreman-Mackey, D. 2018, ApJ, 860, L12
Teague, R., Bae, J., Aikawa, Y., et al. 2021, ApJS, 257, 18
van der Marel, N., & Mulders, G. D. 2021, AJ, 162, 28
van der Plas, G., van den Ancker, M. E., Waters, L. B. F. M., & Dominik, C. 2015, A&A, 574, A75
van der Plas, G., Ménard, F., Canovas, H., et al. 2017, A&A, 607, A55
Villenave, M., Ménard, F., Dent, W. R. F., et al. 2020, A&A, 642, A164
Virtanen, P., Gommers, R., Oliphant, T. E., et al. 2020, Nat. Methods, 17, 261
Walsh, C., Juhász, A., Meeus, G., et al. 2016, ApJ, 831, 200
Waters, L. B. F. M., & Waelkens, C. 1998, ARA&A, 36, 233
Woitke, P., Kamp, I., Antonellini, S., et al. 2019, PASP, 131, 064301
Zacharias, N., Monet, D. G., Levine, S. E., et al. 2004, Am. Astron. Soc. Meeting Abstracts, 205, 48.15

Appendix A: Spectral energy distributions

Figure A.1 presents the SEDs of the eight Herbig disks. The main distinction between the group I and group II disks is clear: group I disks have extra emission at mid-far IR wavelengths, while group II disks only decrease in emission with increasing wavelength.

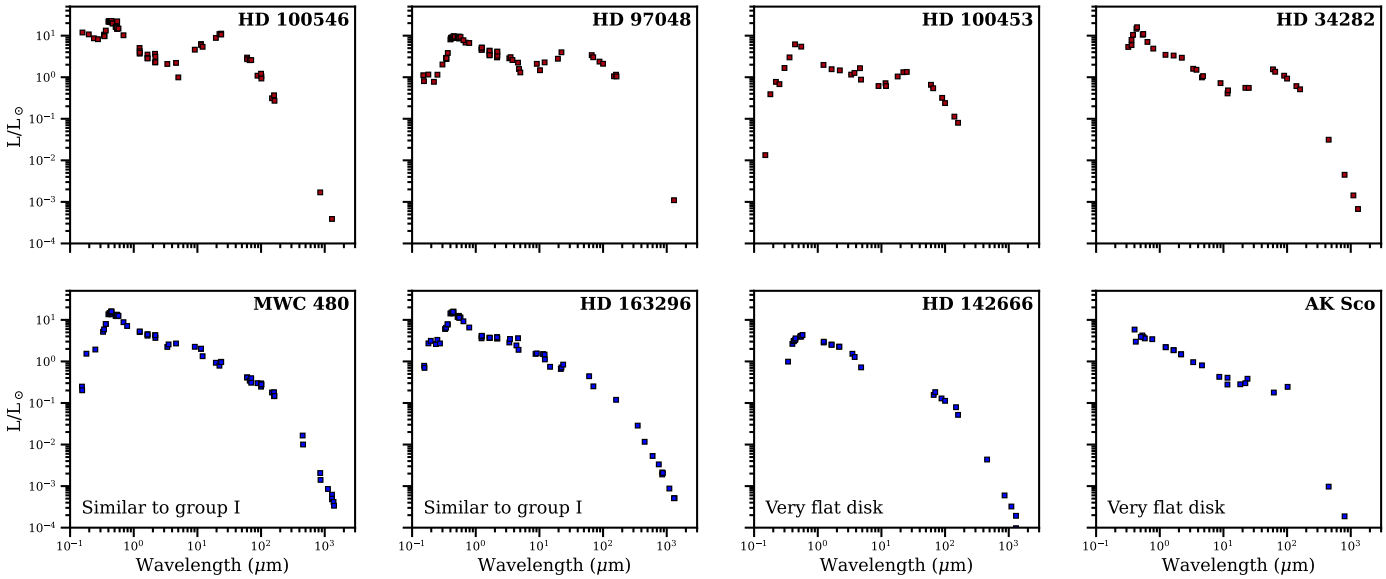

Fig. A.1: Spectral energy distributions (SEDs) of the eight disks. The top and bottom rows show the SEDs of the group I and group II sources, respectively. The SEDs of HD 100546, HD 97048, MWC 480, HD 163296, and HD 142666 are from the DIANA project (Woitke et al. 2019). The SEDs of HD 100453 and HD 34282 are from Khalafinejad et al. (2016). Lastly, the SED of AK Sco is compiled from the following sources: ESA (1997); Hindsley & Harrington (1994); Zacharias et al. (2004); Gaia Collaboration (2020); Ishihara et al. (2010); Cutri & et al. (2012); Jensen et al. (1996). The SEDs of HD 100453, HD 34282, and AK Sco have been dereddened using the `Astropy` affiliated package `dust_extinction` with $R_V = 3.1$ (Bessell 1979) and a visual extinction (A_V) from Guzmán-Díaz et al. (2021).

Appendix B: Channel maps

Figures B.1 to B.8 show the ^{12}CO J = 2–1 channel maps used in this work together with the hand-drawn masks. The masks have been made by carefully identifying the emitting regions visually. We did not use the central channels nor the first and last channels because a horizontal extent and a separation between the far side and the nearside is necessary to extract the heights.

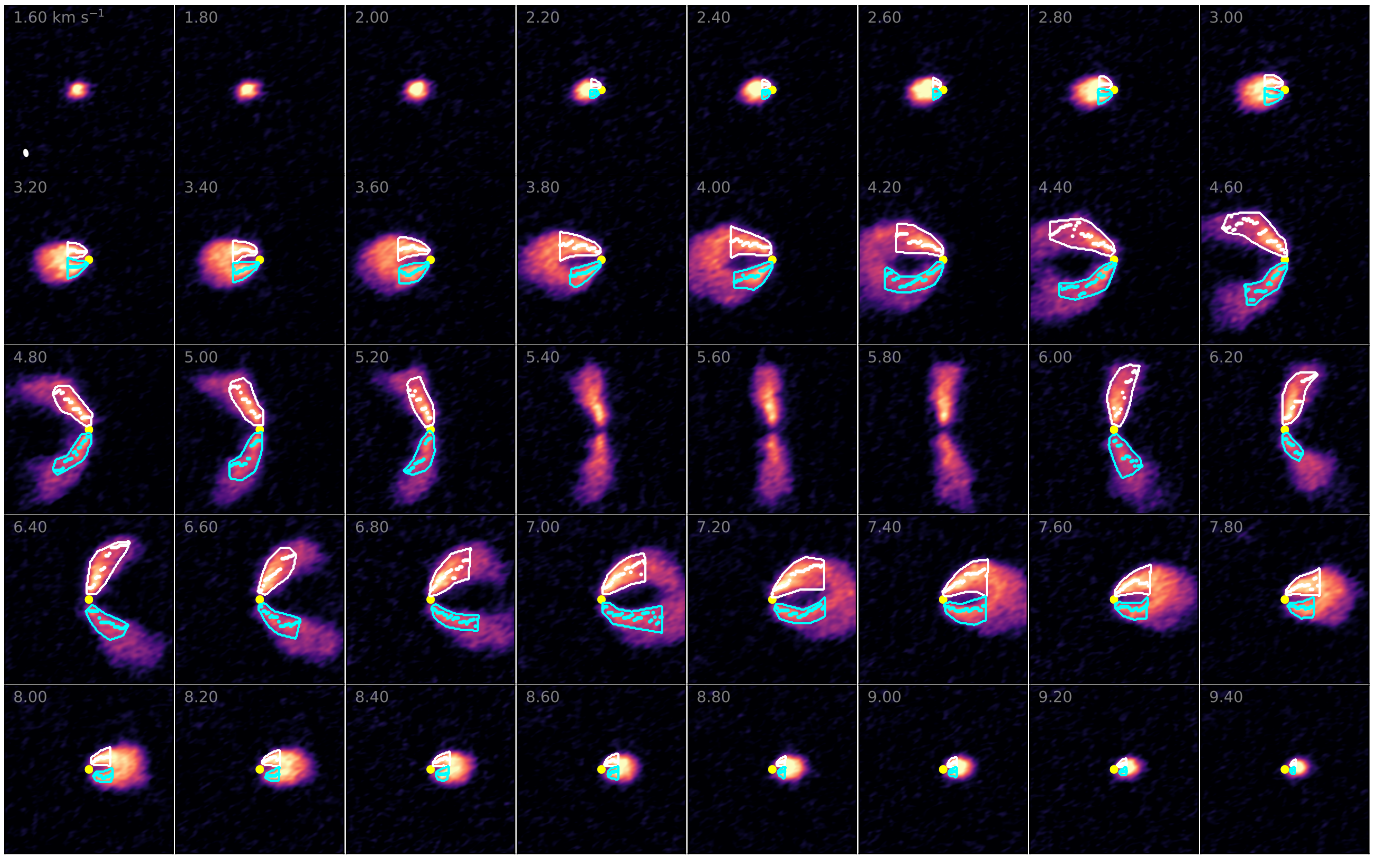

Fig. B.1: ^{12}CO channel maps of HD 100546. The white and blue lines show the outlines of the hand-drawn masks of the far sides and the nearside, respectively. The white and blue scatter show the corresponding extracted points. The yellow circle denotes the position of the star. To make the fainter parts more visible, a power-law normalization was used. On each panel, the channel velocity in km s^{-1} is indicated in the top-left corner. The beam size is shown in the bottom-left corner of the first panel.

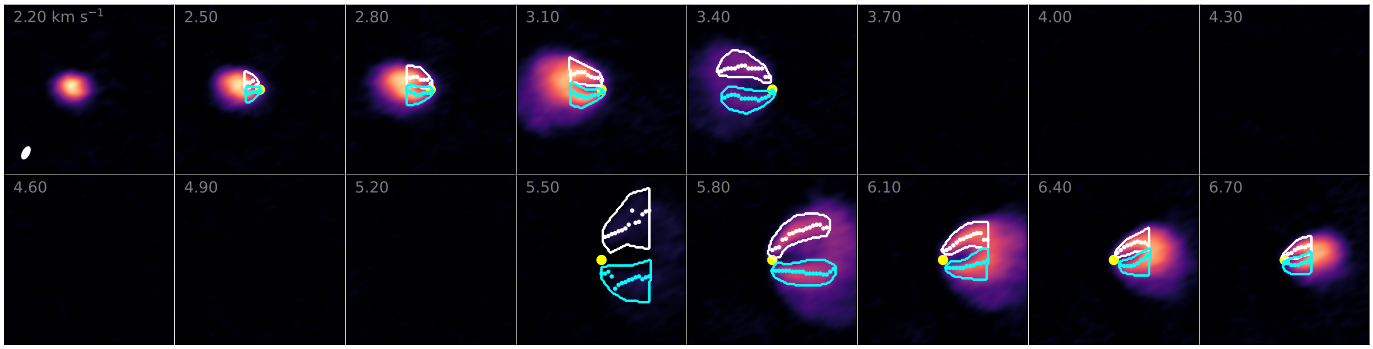

Fig. B.2: Similar to Fig. B.1, but for HD 97048.

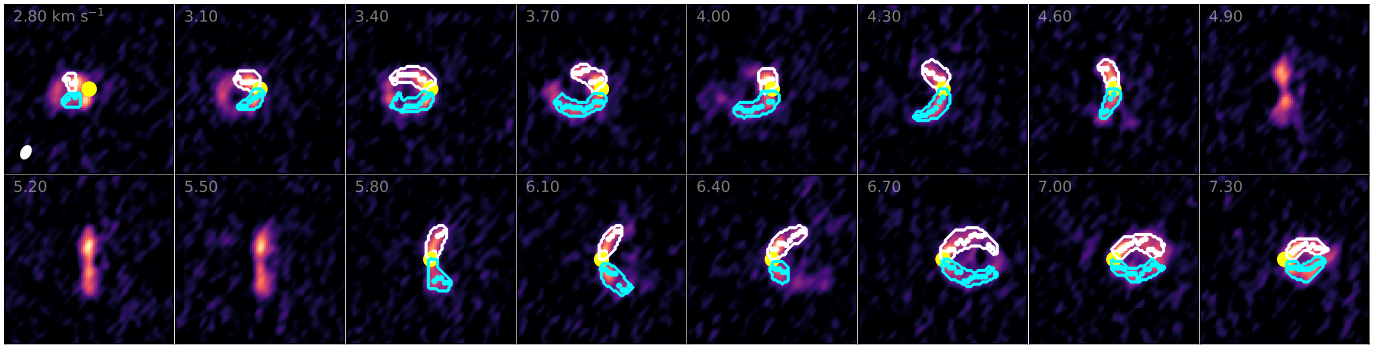

Fig. B.3: Similar to Fig. B.1, but for HD 100453.

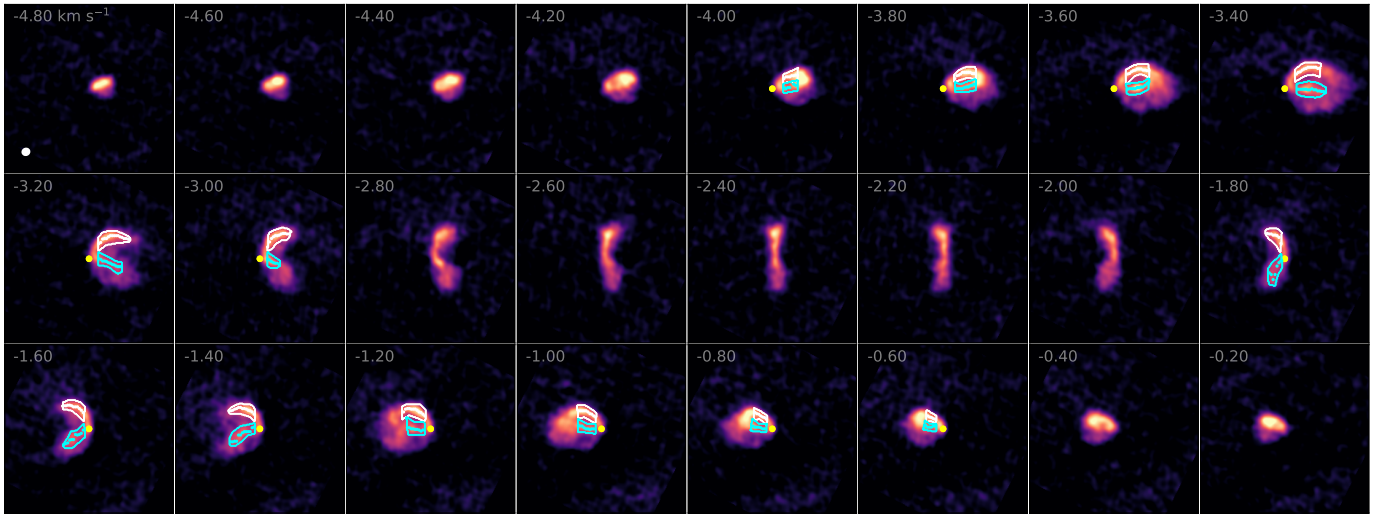

Fig. B.4: Similar to Fig. B.1, but for HD 34282.

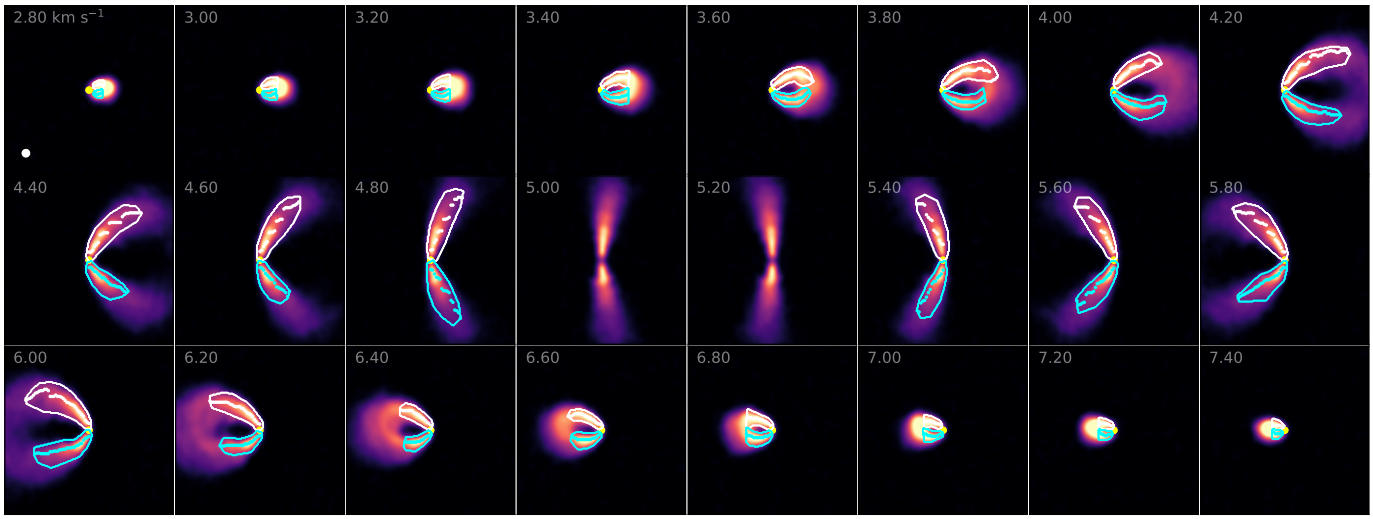

Fig. B.5: Similar to Fig. B.1, but for MWC 480.

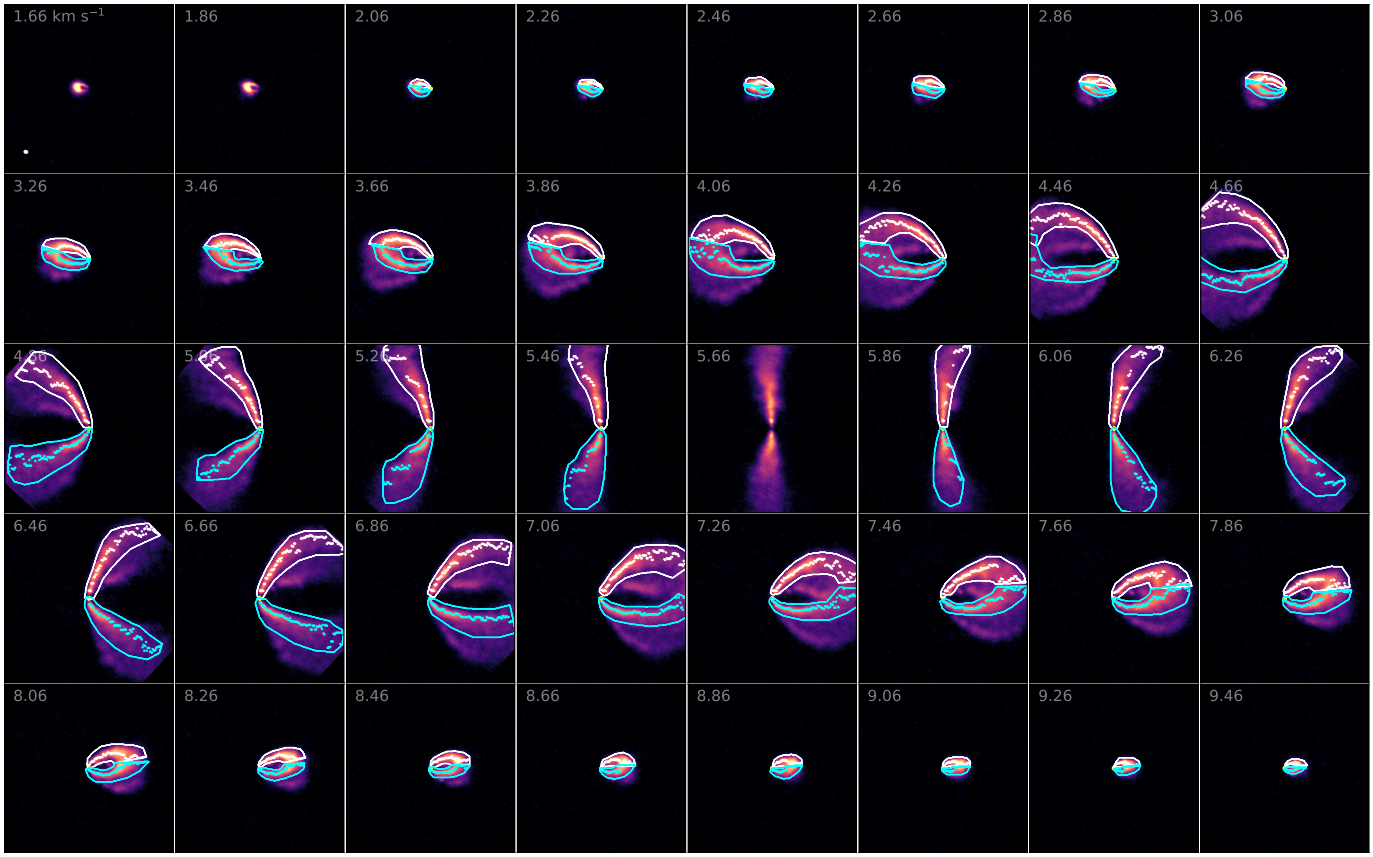

Fig. B.6: Similar to Fig. B.1, but for HD 163296.

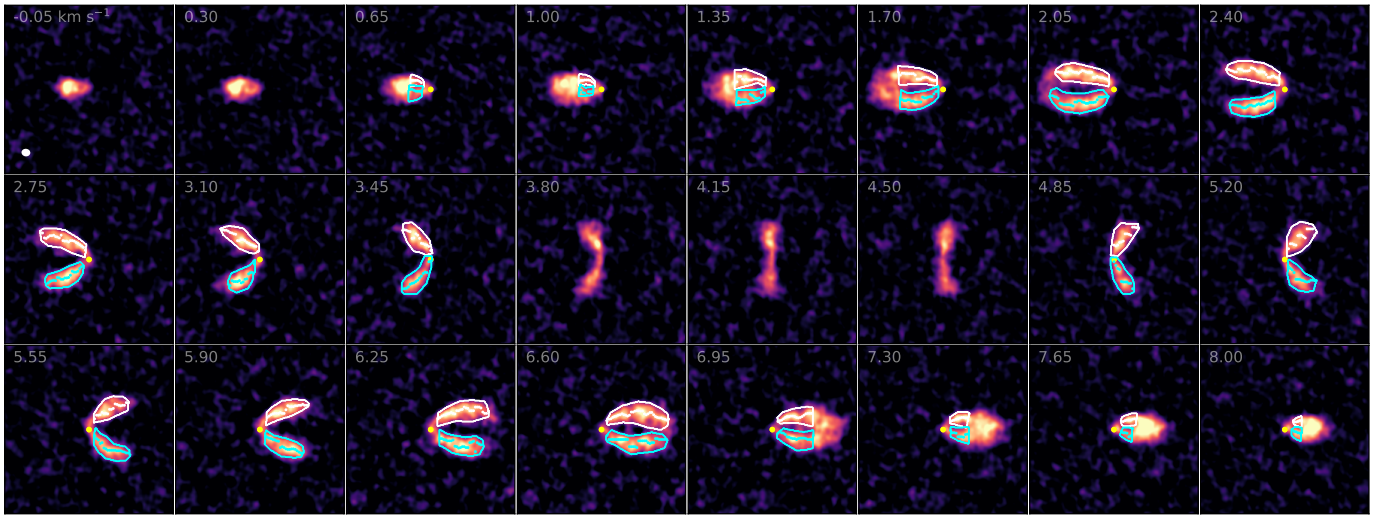

Fig. B.7: Similar to Fig. B.1, but for HD 142666.

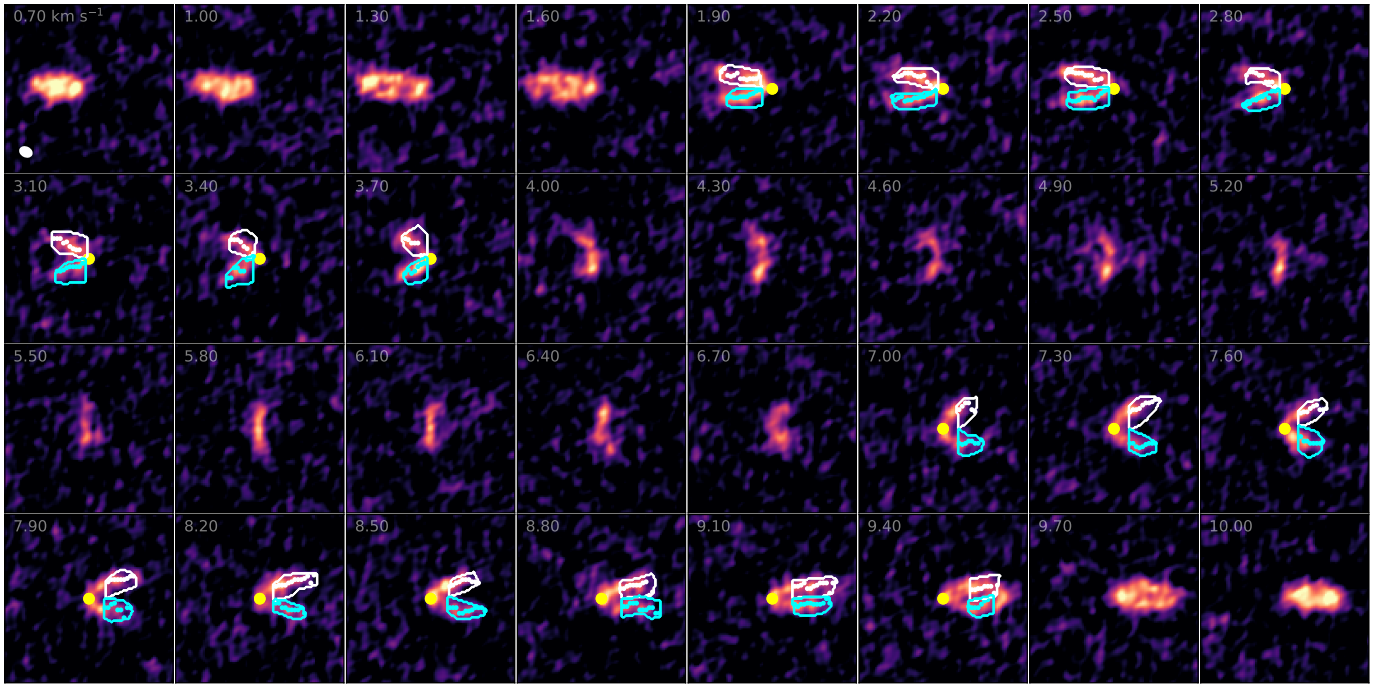

Fig. B.8: Similar to Fig. B.1, but for AK Sco.

Appendix C: Velocity maps

Fig. C.1 shows the moment 1 maps of the disks made with `bettermoments` (Teague et al. 2018) clipped at an S/N of 3. In these figures, the alignment of the redshifted and blueshifted sides provide an additional indication of how vertically extended a disk is. At high enough inclinations, the largest velocities at a particular separation curve with the vertical height of the disk. Hence, if the redshifted and blueshifted sides are aligned opposite to each other, the disk is flat, as seen in the HD 142666 and AK Sco disks. In contrast, a v shape indicates a vertically extended disk, as seen in HD 34282 and HD 163296.

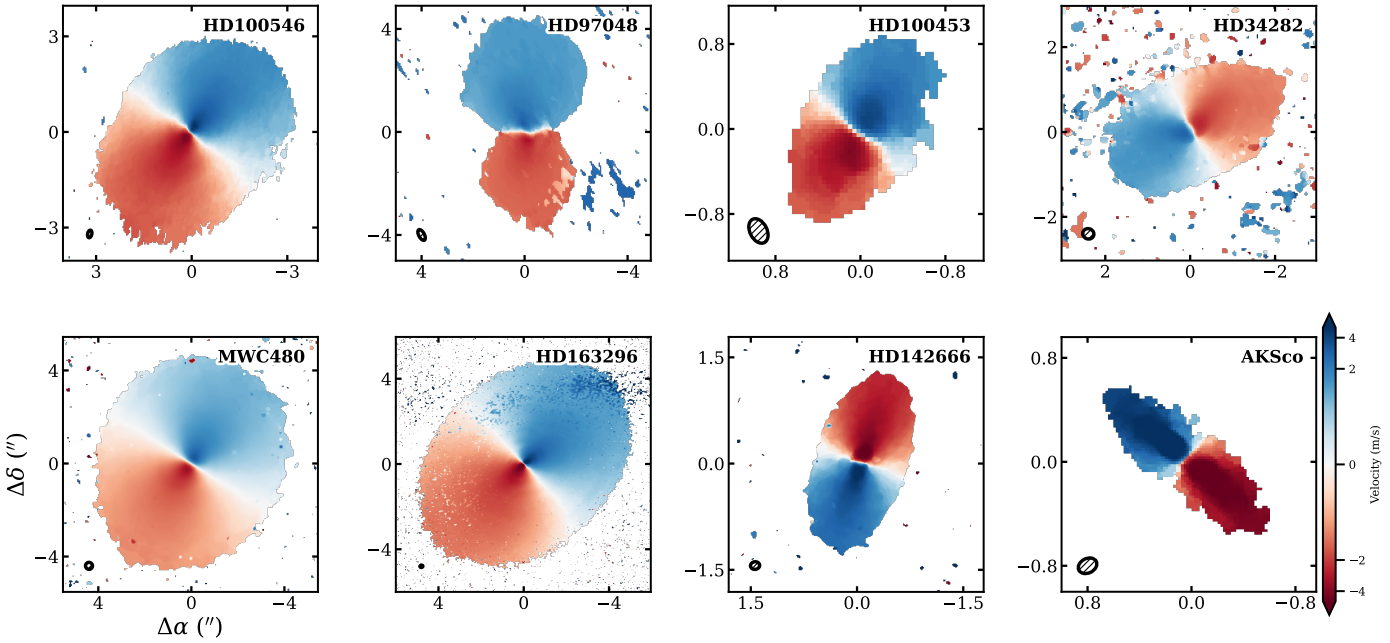

Fig. C.1: Moment one (intensity weighted average velocity) maps of the eight disks. The top and bottom rows show the group I and II disks, respectively. The color bar is centered on their respective system velocities. Each map is clipped at an S/N of 3. The size of the beam is shown in the bottom-right corner.